# Unexpected thermal conductivity enhancement in pillared graphene nanoribbon with isotopic resonance

Dengke Ma, Xiao Wan, and Nuo Yang*

*State Key Laboratory of Coal Combustion, Huazhong University of Science and Technology (HUST), Wuhan 430074, P. R. China and Nano Interface Center for Energy (NICE), School of Energy and Power Engineering, Huazhong University of Science and Technology (HUST), Wuhan 430074, P. R. China*

(Received 21 September 2018; revised manuscript received 27 November 2018; published 26 December 2018)

Wave effects of phonons play an important role in modulating thermal transport in nanostructures. In this paper, we calculated the thermal conductivity of a species of graphene nanoribbon phononic metamaterials (GNPM), pillared graphene nanoribbon, through nonequilibrium molecular dynamics. Interestingly, it is found that the thermal conductivity of GNPM is enhanced by isotopic resonance at pillars, which is in contrast to the reduction by isotopic doping. Furthermore, mode-analysis and atomic Green's function calculations reveal that the mechanism of enhancement originates from the broken hybridization. Additionally, we calculated the effects of the ribbon's width and pillars' height on the thermal conductivity of GNPM. The isotopic resonance provides a mechanism to manipulate phonon transport in nanostructures.

DOI: 10.1103/PhysRevB.98.245420

## I. INTRODUCTION

Nanoribbons, which are patterned as thin strips of two-dimensional materials, have attracted great attention due to their outstanding properties that differ from their two-dimensional counterparts [1]. Graphene nanoribbon (GNR) can open the bandgap in semimetal graphene and give it the potential to be applied in transistors, photovoltaics, and valleytronics [1]. It has been demonstrated that the electric [1], magnetic [2], and spin-related [3] properties of GNR can be modulated by engineering the ribbon width and the edge configuration. The thermal properties of GNR are also very important both for improving the performance and reliability of devices and fundamental understanding of the physics in low-dimensional system [4,5].

The thermal conductivity of pristine GNR with different length and width are studied by molecular dynamical simulation [6] and experiment [7]. To manipulate thermal properties of GNR, different strategies have been put forward. The most commonly exercised approaches are based on the particle nature of phonon. It is found that edge roughness, [8–11] porous [12,13], folding, [14] hydrogen termination [15], random defect, and doping [16–19] would effectively tune the thermal conductivity of GNR. By utilizing edge and folding effect, thermal diode [20] and adjustable thermal resistor [21] can be realized in asymmetric and folded GNR, respectively.

Another way of manipulating thermal properties of GNR is utilizing the wave nature of phonon [22,23], which can be realized in two distinct ways. The first is a phononic crystal which is based on Bragg scattering. By introducing periodic pores [24–27] or isotopes [28,29] in GNR, wave interferences occur and provide a unique frequency band structure with the possibility of band gaps [30,31]. This would hugely reduce the thermal conductivity of GNR [24,25,28,29]. The second is phononic metamaterial (PM) which is based on local resonant hybridization [32–34]. The local resonant hybridization has the advantage to block phonon transport, and is not expected to scatter electrons [32,35]. What is more, the occurring of resonant hybridization does not need the structure to be periodic [36]. This simplifies the synthesis of PM.

Previous researches about local resonant hybridization are focused on silicon based three dimensional nanostructures. [32,35–37] In this paper, we perform nonequilibrium molecular dynamical (NEMD) simulation to study the thermal conductivity of graphene nanoribbon phononic metamaterials (GNPM, shown in Fig. 1). The dependence of thermal conductivity on both ribbon width ($W$) and pillar height ($H_P$) is studied. Moreover, by introducing isotopic atoms to replacing $C^{12}$ in pillars [as shown in the inset of Fig. 2 (b)] the isotopic engineering effect on thermal conductivity is also performed. (To differ from isotopic doping, we term it isotopic replacing.) Mode-analysis (lattice dynamics) and atomistic Green's function (AGF) calculations are carried out to reveal the underlying physical mechanism.

## II. STRUCTURE AND METHODS

GNPM is made up of GNR with pillars on two sides (shown in Fig. 1). The pillars serve as resonators [32]. The GNPM has been successfully fabricated of atomically precise on experiment [3]. The lattice constant (a) and thickness (d) of GNPM are 0.1438 nm and 0.334 nm, respectively. Throughout this paper, the total length ($L$), $L_1$, $L_2$, and $L_P$ are fixed as 10 nm (80 layers), 1.62, 0.87, and 0.62 nm, respectively.

NEMD simulations in this paper are performed using the LAMMPS package [38–42] with the optimized Tersoff potential, which has successfully reproduced the thermal properties of graphene [19,43,44]. The detailed parameters of the

*nuo@hust.edu.cn

 

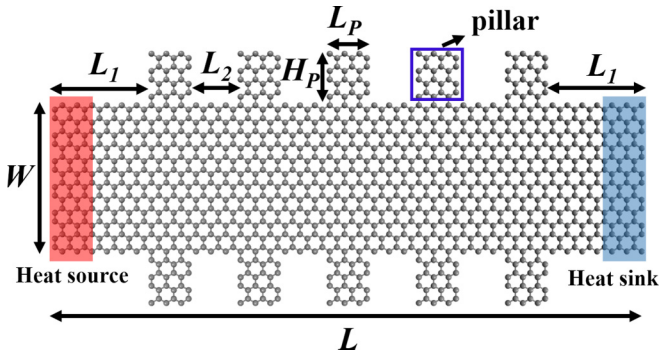


FIG. 1. Schematic picture of the GNPM which is made up of GNR with pillars on two sides. The fixed (free) boundary conditions are applied in longitudinal (transverse) direction. The total length ($L$) is fixed as 10 nm (80 layers). $L_1$, $L_2$, and $L_P$ are fixed as 1.62, 0.87, and 0.62 nm, respectively.

optimized Tersoff potential are shown in Table S1 of the Supplemental Material (SM) [45]. The fixed (free) boundary conditions are applied in the longitudinal (transverse) direction. In order to establish a temperature gradient along the longitudinal direction, the system is coupled with Langevin thermostats [28] at the 3rd to 6th and ($N$-6) th to ($N$-3) th layers with 310 and 290 K, respectively. Atoms at the boundaries (the 1st to 2nd and $(N-1)$ th to $N$ th layers) are fixed.

The equations of motions are integrated by the velocity Verlet method with a time step of 0.5 fs. Initially, the system is relaxed in the NPT ensemble (constant number of atoms, pressure and temperature) at 300 K and 0 bar for 1 ns, followed by relaxation under the NVE ensemble (constant number of atoms, volume and total energy) for 2.5 ns. After that, a time average of the temperature and heat current is performed for 10 ns. The results presented here are averaged over six independent simulations with different initial conditions.

The temperature gradient is obtained by linear fitting to the local temperature, excluding the temperature jumps at the two ends. The thermal conductivity is calculated based on Fourier's Law,

$$\kappa = -\frac{J}{W \cdot d \cdot \nabla T}, \tag{1}$$

where $J$ denotes the heat current transported from the hot bath to the cold bath, $W$ is the width, $d$ is the thickness, and $\nabla T$ is the temperature gradient along the longitudinal direction. It should be noted that when calculating the cross section area of GNPM, we use the effective width ($W$). The height of the pillar part is not included. The temperature $T_{MD}$ is calculated from the kinetic energy of atoms ($3Nk_BT_{MD}/2 = \sum_i m_i v_i^2/2$).

## III. RESULTS AND DISCUSSION

We first calculate the thermal conductivity of GNPM ($\kappa_{\mathrm{GNPM}}$) with different $W$, and compare them with the thermal conductivity of corresponding GNR ($\kappa_{\mathrm{GNR}}$). Here, the $H_P$ is fixed as 0.86 nm. Figure 2(a) shows the relative thermal conductivity ($\kappa_{\mathrm{GNPM}}/\kappa_{\mathrm{GNR}}$). When $W$ increases from 0.86 to 4.32 nm, the relative thermal conductivity (black dot) increases from 0.27 to 0.43. This means the introduction of pillars (structural resonance) greatly reduce the $\kappa_{\mathrm{GNR}}$.

To understand the underlying physical mechanism and explicitly show the pillar effect, we carry out a vibrational mode-analysis of phonons in GNR and GNPM. As shown in the phonon dispersion relations of GNR [Fig. 3(a)] and GNPM [Fig. 3(b)], there are many flat bands in GNPM which is the signature of local resonance [32,35,36,46]. These resonant modes hybridize with the propagating modes across the ribbon. It will hinder the transport of propagating modes and reduce their group velocities [32,35]. As shown in Fig. 3(c), the group velocities of GNPM (red dot) are quite lower than those of GNR (blue dot) in the whole frequency range.

Since the reduction of thermal conductivity is due to the resonant hybridization wave effect, the increase of relative thermal conductivity with the increasing of $W$ is easy to understand. As the size of the pillars keeps the same, the resonant modes do not change, while the number of propagating modes increases as $W$ increases. As a result, the proportion of

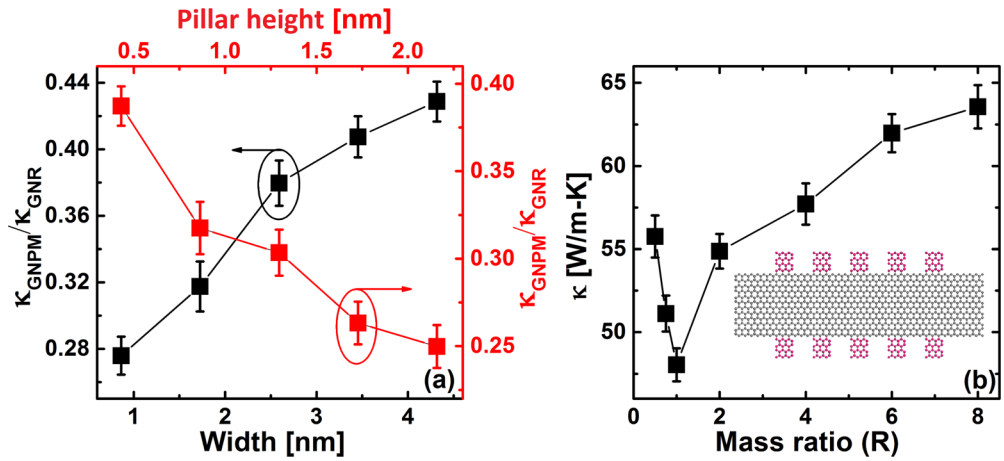


FIG. 2. (a) Thermal conductivity of GNPM versus the width ($W$) and pillar height ($H_P$). (b) Thermal conductivity of isotopic doped GNPM with different mass ratio ($R$). Here, $R$ is defined as $R = M/12$, where $M$ is the atomic mass of the isotope of C in the pillar (red atoms). The mass of atoms in the ribbon part (gray atoms) is kept as 12. The inset is the schematic picture of isotopic doped GNPM.

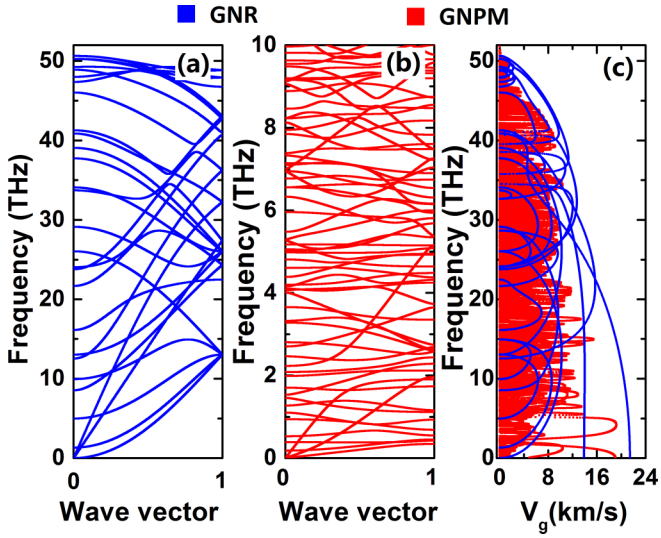


FIG. 3. The phonon dispersion relationship of (a) GNR and (b) GNPM. (c) The group velocity of GNR (blue dot) and GNPM (red dot).

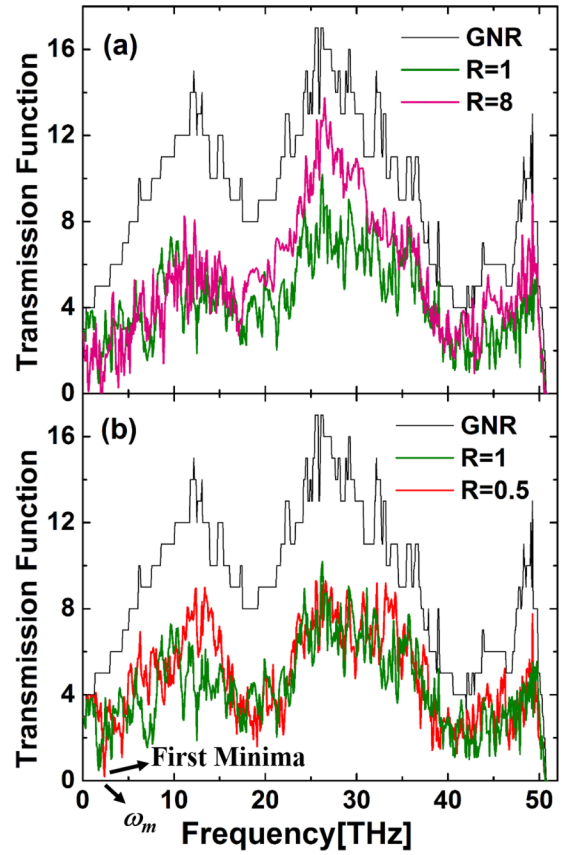


FIG. 4. The phonon transmission function of GNR (black line), GNPM ($R = 0.5$) (red line), GNPM ($R = 1$) (green line), and GNPM ($R = 8$) (pink line).

propagating modes that can hybridize with resonant modes decreases. This leads to the increasing of relative thermal conductivity.

We also calculate the $\kappa_{\mathrm{GNPM}}$ with different $H_P$, while $W$ is fixed as 1.73 nm. As shown in Fig. 2(a) (red dots), when $H_P$ increases from 0.43 to 2.16 nm, the $\kappa_{\mathrm{GNPM}}/\kappa_{\mathrm{GNR}}$ decreases from 0.39 to 0.25. As here the $\kappa_{\mathrm{GNR}}$ does not change, it means the $\kappa_{\mathrm{GNPM}}$ decreases with $H_P$ increases. This tendency is consistent with observations in silicon based PM [47]. One reason is that increasing $H_P$ increases the number of resonant modes. Another reason is that larger $H_P$ will induce resonant modes with lower frequency, and form more hybridization in low frequency [35]. Generally, the low frequency modes contribute more to the thermal conductivity.

The isotopic engineering is an effective way to block phonon transport and reduce thermal conductivity [48–50]. Besides the dependence of $\kappa_{\mathrm{GNPM}}$ on system size ($W$ and $H_P$), one of the isotopic engineering effects, isotopic replacing, is also investigated. There are only 15 known isotopes of C, whose atomic mass changes only from 8 to 22. Artificial C isotopic atoms here are used to explore the mass influence on the thermal transport, and can be regarded as other atoms [51], such as $^{56}$Fe [51]. When there are other kinds of atoms, the system is more complicated. That is, the mass is not the only factor involved. The bond strength and lattice relaxations must play a role, which is not studied in this letter. The inset of Fig. 2(b) shows the structure of isotopic replaced GNPM. Here, we change the mass of atoms in the pillars (red atoms), and keep the mass of atoms in the ribbon part unchanged (gray atoms). The bottom-up approach is one of the best ways to fabricate the isotopic replaced GNPM. For example, the isotopic replaced GNPM can be obtained by fusing segments made from two different molecular building blocks with different atomic mass (e.g., 12 and 22) [52]. Moreover, if using different kind of atoms, e.g. Fe, instead of isotopic doped C, the isotopic replaced GNPM can be fabricated by the multistep method. This method has been widely used in fabricating branched nanowire heterostructures [53].

We define a parameter, mass ratio ($R$), as $R = M/12$, where $M$ is the atomic mass of the isotope of C in the pillars. The $W$ and $L_P$ are fixed as 1.73 and 0.86 nm, respectively. As shown in Fig. 2(b), the minimum $\kappa_{\mathrm{GNPM}}$ is observed when $R$ equals 1, which means there is no isotopic atoms. When $R$ decreases from 1 to 0.5, the $\kappa_{\mathrm{GNPM}}$ increases from 48.0 to 55.8 $\mathrm{Wm^{-1}\,K^{-1}}$. When $R$ increases from 1 to 8, the $\kappa_{\mathrm{GNPM}}$ increases from 48.0 to 63.6 $\mathrm{Wm^{-1}\,K^{-1}}$. This means the isotopic replaced GNPM with lighter or heavier isotopic atoms both increase the $\kappa_{\mathrm{GNPM}}$ surprisingly.

It is well-known that isotopic engineering generally reduces thermal conductivity [48,49], which has also been observed in previous studies on GNR [17,28,29]. To understand the unexpected increase of $\kappa_{\mathrm{GNPM}}$ by isotopic replacing, we calculate the phonon transmission for GNR and GNPM ($R =$ 0.5, 1, 8) through the AGF method [54]. (The details of AGF calculation is given in SM II [45].) As shown in Fig. 4(a), the transmission function of GNR (black line) is larger than that of GNPM (green line) in the whole frequency range, which also serves as evidence for the reduction of thermal conductivity by resonant hybridization. What is more important, the transmission function for GNPM with isotopic replacing ($R =$ 0.5 and 8) are larger than pristine GNPM ($R = 1$) in wide frequency ranges. This implies the enhancement in thermal

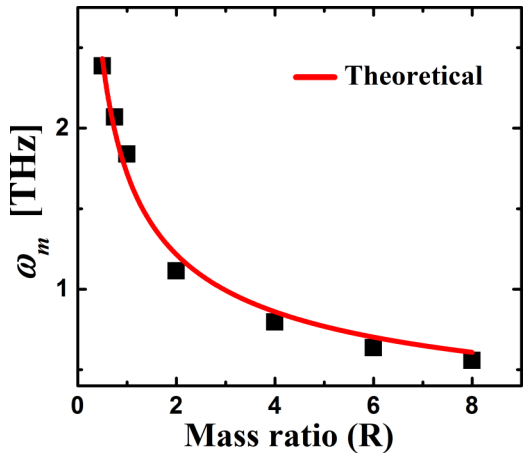


FIG. 5. The frequency ($\omega_m$) of the first transmission function minima versus mass ratio.

conductivity. The phonon group velocity for the cases with different pillar mass is given in SM III [45].

The unexpected facilitated phonon transport by isotopic replacing is due to the mechanism of broken hybridization. The phonon hybridizations in GNPM mean the interactions between resonant phonon modes in the pillars and the propagated phonon modes across the ribbon. The hybridization occurs when two phonon modes with the same polarization located on different objects are coupled at the same frequency [46]. The frequency has an inverse relationship with the atomic mass and the eigenvalue of frequency is shifted by isotopic engineering [55]. That is, for pillars with heavier (lighter) isotopic atoms, the frequencies of resonant modes are lower (higher) comparing to those with $C^{12}$ atoms, whereas the propagating modes in the ribbon stay the same. Then, it induces the mismatch between the resonant modes and propagating modes by isotopic engineering, which will break and decrease the original hybridization and facilitate phonon transport. The shift of resonant modes can be observed from Fig. 4. For example, the frequency of the first transmission function minima is 1.84 THz, corresponding to $R = 1$. When using heavier (lighter) isotopic atoms in pillars, the frequency for $R = 8 (R = 0.5)$ is 0.56 THz (2.39 THz), which is lower (higher) than that for $R = 1$.

To quantitatively show the isotopic resonance effect on the resonant hybridization, we focus on the shifting of the frequency ($\omega_m$) of the first transmission function minima (shown in Fig. 4) by changing the mass of isotopic atoms. As shown in Fig. 5, the $\omega_m$ decreases with the increasing of the mass ratio (black dot), which means the first transmission function minima shifts to low frequency gradually with the isotopic atomic mass increases. The relationship between the phonon frequency and the atomic mass can be approximated as $\omega \sim m^{-0.5}$ [55]. We use the formula $\omega_m = aR^{-0.5}$ ($a$ is a constant) to fit the simulation dates, as shown in Fig. 5, the theoretical formula (red line) matches well with the simulation dates (black dot). This result further validates the mechanism behind broken hybridization.

To make a clear understanding about the enhancement of thermal conductivity, we compare the mechanism of isotopic resonance with isotopic doping. The isotopic engineering by random or periodic doping generally leads to phonon localization [17], introduces a band gap [28,29,48] or increases phonon scattering [49], which blocks phonon transport and reduces thermal conductivity. Here, the isotopic atoms are applied on the resonant pillars, which causes the shifts of resonant frequencies. Then, it induces the mismatch between the resonant modes and propagating modes, which breaks the original hybridization. So, the isotopic resonance facilitates phonon transport and enhances thermal conductivity of GNPM.

## IV. CONCLUSION

In summary, we have calculated the thermal conductivity of graphene nanoribbon phononic metamaterials (GNPM) via the NEMD simulation. It is interesting that isotopic resonance by lighter and heavier isotopic atoms in pillars can both enhance thermal conductivity of GNPM. For pillars with lighter isotopic atoms, when mass ratio ($R$) decreases from 1 to 0.5, the $\kappa_{\mathrm{GNPM}}$ increases from 48.0 to 55.8 $\mathrm{Wm^{-1}\,K^{-1}}$. Whereas for pillars with heavier isotopic atoms, when $R$ increases from 1 to 8, the $\kappa_{\mathrm{GNPM}}$ increases from 48.0 to 63.6 $\mathrm{Wm^{-1}\,K^{-1}}$. After phonon mode analysis (lattice dynamics) and AGF calculation, it is concluded that the local resonant hybridization wave effect governs phonon transport in GNPM. By introducing heavier (lighter) isotopic atoms to replacing $C^{12}$ atoms in pillars, the frequencies of resonant modes are decreased (increased), whereas the propagating modes across the ribbon stay the same. It induces the mismatch between the resonant modes and propagating modes, which breaks and decreases the original hybridization and facilitates phonon transport. Additionally, it is also found that when pillar height ($H_P$) increases from 0.43 to 2.16 nm, the $\kappa_{\mathrm{GNPM}}/\kappa_{\mathrm{GNR}}$ decreases from 0.39 to 0.25. When ribbon width ($W$) increases from 0.86 to 4.32 nm, the $\kappa_{\mathrm{GNPM}}/\kappa_{\mathrm{GNR}}$ increases from 0.27 to 0.43. This work provides a mechanism for future engineering on phonon transport in GNR and other nanoribbon based structures.

## ACKNOWLEDGMENTS

N.Y. is sponsored by National Natural Science Foundation of China (Grants No. 51576076 and No. 51711540031), Natural Science Foundation of Hubei Province (No. 2017CFA046), and Fundamental Research Funds for the Central Universities No. (2016YXZD006). The authors thank the National Supercomputing Center in Tianjin [TianHe-1 (A)] and the China Scientific Computing Grid (ScGrid) for providing assistance in computations.

The authors declare no competing financial interests.

[1] M. Liang, W. Jinlan, and D. Feng, ChemPhysChem **14**, 47 (2013).

[2] E.-j. Kan, Z. Li, J. Yang, and J. G. Hou, J. Am. Chem. Soc. **130**, 4224 (2008).

[3] P. Ruffieux, S. Wang, B. Yang, C. Sánchez-Sánchez, J. Liu, T. Dienel, L. Talirz, P. Shinde, C. A. Pignedoli, D. Passerone, T. Dumslaff, X. Feng, K. Müllen, and R. Fasel, Nature (London) **531**, 489 (2016).

[4] D. G. Cahill, P. V. Braun, G. Chen, D. R. Clarke, S. Fan, K. E. Goodson, P. Keblinski, W. P. King, G. D. Mahan, and A. Majumdar, Appl. Phys. Rev. **1**, 011305 (2014).

[5] T. Ouyang, E. Jiang, C. Tang, J. Li, C. He, and J. Zhong, J. Mater. Chem. A **6**, 21532 (2018).

[6] J. Shiomi and S. Maruyama, Int. J. Thermophys. **31**, 1945 (2010).

[7] X. Xu, L. F. C. Pereira, Y. Wang, J. Wu, K. Zhang, X. Zhao, S. Bae, C. Tinh Bui, R. Xie, J. T. L. Thong, B. H. Hong, K. P. Loh, D. Donadio, B. Li, B. Özyilmaz, Nat. Commun. **5**, 3689 (2014).

[8] G. Xie, Z. Ju, K. Zhou, X. Wei, Z. Guo, Y. Cai, and G. Zhang, Npj Comput. Mater. **4**, 21 (2018).

[9] S. Xiong, J. Ma, S. Volz, and T. Dumitrică, Small **10**, 1756 (2014).

[10] J. Maire, R. Anufriev, T. Hori, J. Shiomi, S. Volz, and M. Nomura, Sci. Rep. **8**, 4452 (2018).

[11] C. Shao, Q. Rong, N. Li, and H. Bao, Phys. Rev. B **98**, 155418 (2018).

[12] T. Feng and X. Ruan, Carbon **101**, 107 (2016).

[13] B.-Y. Cao, W.-J. Yao, and Z.-Q. Ye, Carbon **96**, 711 (2016).

[14] N. Yang, X. Ni, J.-W. Jiang, and B. Li, Appl. Phys. Lett. **100**, 093107 (2012).

[15] W. J. Evans, L. Hu, and P. Keblinski, Appl. Phys. Lett. **96**, 203112 (2010).

[16] S. Chen, Q. Wu, C. Mishra, J. Kang, H. Zhang, K. Cho, W. Cai, A. A. Balandin, and R. S. Ruoff, Nat. Mater. **11**, 203 (2012).

[17] J. W. Jiang, J. H. Lan, J. S. Wang, and B. W. Li, J. Appl. Phys. **107**, 054314 (2010).

[18] W. Ma, Y. Liu, S. Yan, T. Miao, S. Shi, Z. Xu, X. Zhang, and C. Gao, Nano Res. **11**, 741 (2018).

[19] S. Hu, J. Chen, N. Yang, and B. Li, Carbon **116**, 139 (2017).

[20] N. Yang, G. Zhang, and B. Li, Appl. Phys. Lett. **95**, 033107 (2009).

[21] Q. Song, M. An, X. Chen, Z. Peng, J. Zang, and N. Yang, Nanoscale **8**, 14943 (2016).

[22] J. Maire, R. Anufriev, R. Yanagisawa, A. Ramiere, S. Volz, and M. Nomura, Sci. Adv. **3**, e1700027 (2017).

[23] L. Feng, T. Shiga, H. Han, S. Ju, Y. A. Kosevich, and J. Shiomi, Phys. Rev. B **96**, 220301 (2017).

[24] L. Yang, J. Chen, N. Yang, and B. Li, Int. J. Heat Mass Tran. **91**, 428 (2015).

[25] S. Hu, M. An, N. Yang, and B. Li, Nanotechnology **27**, 265702 (2016).

[26] S. Hu, Z. Zhang, P. Jiang, J. Chen, S. Volz, M. Nomura, and B. Li, J. Phys. Chem. Lett. **9**, 3959 (2018).

[27] L. Cui, S. Shi, Z. Li, G. Wei, and X. Du, Phys. Chem. Chem. Phys. **20**, 27169 (2018).

[28] T. Ouyang, Y. P. Chen, K. K. Yang, and J. X. Zhong, Europhys. Lett. **88**, 28002 (2009).

[29] X. Mu, T. Zhang, D. B. Go, and T. Luo, Carbon **83**, 208 (2015).

[30] S. Volz, J. Shiomi, M. Nomura, and K. Miyazaki, J. Therm. Sci. Tec. Jpn. **11**, JTST0001 (2016).

[31] G. Xie, D. Ding, and G. Zhang, Adv. Phys.: X **3**, 1480417 (2018).

[32] B. L. Davis and M. I. Hussein, Phys. Rev. Lett. **112**, 055505 (2014).

[33] S. Xiong, D. Selli, S. Neogi, and D. Donadio, Phys. Rev. B **95**, 180301 (2017).

[34] R. Anufriev and M. Nomura, Phys. Rev. B **95**, 155432 (2017).

[35] S. Xiong, K. Sääskilahti, Y. A. Kosevich, H. Han, D. Donadio, and S. Volz, Phys. Rev. Lett. **117**, 025503 (2016).

[36] D. Ma, H. Ding, H. Meng, L. Feng, Y. Wu, J. Shiomi, and N. Yang, Phys. Rev. B **94**, 165434 (2016).

[37] R. Anufriev, R. Yanagisawa, and M. Nomura, Nanoscale **9**, 15083 (2017).

[38] S. Plimpton, J. Comput. Phys. **117**, 1 (1995).

[39] S. Xiong, B. Latour, Y. Ni, S. Volz, and Y. Chalopin, Phys. Rev. B **91**, 224307 (2015).

[40] H. Meng, X. Yu, H. Feng, Z. Xue, and N. Yang, arXiv:1807.04412.

[41] Z. Ding, M. An, S. Mo, X. Yu, Z. Jin, Y. Liao, J. Lu, K. Esfarjani, J. Shiomi, and N. Yang, arXiv:1703.00184.

[42] H. Ding, G. Peng, S. Mo, D. Ma, S. W. Sharshir, and N. Yang, Nanoscale **9**, 19066 (2017).

[43] M. An, Q. Song, X. Yu, H. Meng, D. Ma, R. Li, Z. Jin, B. Huang, and N. Yang, Nano Lett. **17**, 5805 (2017).

[44] D. Ma, H. Ding, X. Wang, N. Yang, and X. Zhang, Int. J. Heat Mass Tran. **108**, 940 (2017).

[45] See Supplemental Material http://link.aps.org/supplemental/10.1103/PhysRevB.98.245420 for additional details about molecular dynamical simulation and atomic Green's function, and phonon group velocity for GNPM with different pillar mass.

[46] H. Honarvar and M. I. Hussein, Phys. Rev. B **97**, 195413 (2018).

[47] Z. Wei, J. Yang, K. Bi, and Y. Chen, J. Appl. Phys. **118**, 155103 (2015).

[48] N. Yang, G. Zhang, and B. Li, Nano Lett. **8**, 276 (2008).

[49] X. Wu, N. Yang, and T. Luo, Appl. Phys. Lett. **107**, 191907 (2015).

[50] X. Li, J. Chen, C. Yu, and G. Zhang, Appl. Phys. Lett. **103**, 013111 (2013).

[51] T. M. Gibbons and S. K. Estreicher, Phys. Rev. Lett. **102**, 255502 (2009).

[52] Y.-C. Chen, T. Cao, C. Chen, Z. Pedramrazi, D. Haberer, D. G. de Oteyza, F. R. Fischer, S. G. Louie, and M. F. Crommie, Nat. Nanotechnol. **10**, 156 (2015).

[53] X. Jiang, B. Tian, J. Xiang, F. Qian, G. Zheng, H. Wang, L. Mai, and C. M. Lieber, Proc. Natl. Acad. Sci. USA **108**, 12212 (2011).

[54] S. Xiong, K. Yang, Y. A. Kosevich, Y. Chalopin, R. D'Agosta, P. Cortona, and S. Volz, Phys. Rev. Lett. **112**, 114301 (2014).

[55] M. T. Dove, *Introduction to Lattice Dynamics* (Cambridge University Press, Cambridge, 1993), pp. 20–22.